Recursive versions of the reassigned scalogram and of the synchrosqueezed Wavelet Transform

Dominique Fourer
UMR STMS (IRCAM - CNRS - UPMC)
1 place Igor Stravinsky, Paris, France
dominique@fourer.fr

François Auger
IREENA - CRTT - LUNAM University
37 boulevard de l'université, Saint-Nazaire, France
francois.auger@univ-nantes.fr

***Abstract*—This paper introduces a new class of mother wavelet functions, based on a specific analysis window which allows a recursive implementation of the Continuous Wavelet Transform (CWT). Using this new transform, we propose to compute a sharpened time-frequency representation by rewording the reassigned scalogram and the (first and second-order) synchrosqueezed CWT. We also propose an extension of the CWT reassignment operators, using the Levenberg-Marquardt algorithm, which can control the energy concentration of a reassigned scalogram through a damping parameter. Thus, our methods provide tools which pave the way of the real-time computation of reversible and almost-ideal time-frequency representations.**

I. Introduction

Most of the real-world signals are non-stationary and made of several time-varying components which can only be revealed by a transform with a narrow time-frequency localization. The Constant Q Transform (CQT) [1] and its related continuous-time transforms such as the S-transform [2] or the Continuous Wavelet Transform (CWT) [3], have shown their superiority over the Short-Time Fourier Transform (STFT) in many application cases, in particular for audio signals, due to their varying frequency resolution which models the signal cochlea transformation [4], [5], [6]. However, the main inconvenience of all these methods compared to the STFT, is that they cannot be efficiently implemented by the means of the Fast Fourier Transform (FFT) algorithm since they use analysis windows of different width, which depend on frequency. A solution was provided by the fast wavelet transform [7] which uses a recursive implementation combined with resampling operations that imposes to each analyzed scale to be a power of two. Therefore, in the proposed work, we first introduce a new mother wavelet function, based on a previously proposed analysis window which leaded us to an efficient STFT implementation through causal recursive filtering [8]. This allows to compute the CWT using a filter-banks without restriction on the scale and using linear combinations involving the previously computed coefficients of the transform with the analyzed signal. Second, we also propose to reword the reassignment operators, its variant involving the Levenberg-Marquardt algorithm [9], and also the first- and the second-order (vertical) recursive synchrosqueezed CWT. All these tools pave the way of a real-time implementation of a sharpened and invertible time-frequency representation (TFR).

This research was supported by the French ANR ASTRES project (ANR-13-BS03-0002-01).

The remainder of the paper is organized as follows. In Section II, we first recall the definition of the CWT with its reassignment operators and its synchrosqueezed transform. In Section III, we introduce a specific mother wavelet function to allow a recursive implementation of the CWT when it is discretized. Then, the proposed methods are evaluated in numerical simulations presented in Section IV. Finally, the paper is concluded with future work directions in Section V.

II. Filter-based CWT, its reassignment and its synchrosqueezing

Let $L^1(\mathbb{R})$ and $L^2(\mathbb{R})$ denote the space of integrable and square integrable functions. Now, we consider a signal $x \in L^1(\mathbb{R})$, and an admissible wavelet $\Psi \in L^2(\mathbb{R})$, which satisfies $0 < C_\Psi = \int_{\mathbb{R}} |F_\Psi(\omega)|^2 \frac{d\omega}{|\omega|} < +\infty$, the Fourier transform of x being expressed as $F_x(\omega) = \int_{\mathbb{R}} x(t)\, \mathrm{e}^{-j\omega t} dt$, with $j^2 = -1$.

Hence, the CWT of a signal x for any time t and any scale s, can be defined as [10]

$$W_x(t,s) = \frac{1}{|s|} \int_{-\infty}^{+\infty} x(\tau) \Psi \left(\frac{\tau - t}{s} \right)^* d\tau, \qquad (1)$$

where z^* is the complex conjugate of z. For this definition, we choose the $\frac{1}{|s|}$ instead of the common $\frac{1}{\sqrt{|s|}}$ for the normalization, since it is more adapted for mode extraction.

Now, if we define each scale as $s = \frac{\omega_0}{\omega}$, with $\omega_0 > 0$, the central frequency of F_Ψ, then Eq. (1) can now be expressed as

$$\mathrm{CW}_x(t,\omega) = \frac{|\omega|}{\omega_0} \int_{-\infty}^{+\infty} x(\tau) \Psi \left(\frac{\omega}{\omega_0}(\tau - t) \right)^* d\tau \qquad (2)$$

$$= \int_{-\infty}^{+\infty} x(\tau)\; g\Big(t - \tau, \frac{\omega_0}{\omega}\Big)\; d\tau. \qquad (3)$$

where $g(t,s) = \frac{1}{|s|} \Psi(-\frac{t}{s})^*$ can be viewed as the impulse response of a filter used in Eq. (3), considered as a convolution product. Hence, a TFR is provided by $|\mathrm{CW}_x(t,\omega)|^2$, which is also called scalogram. However, this quadratic distribution does not belong to the Cohen's class since it is related to the Wigner-Ville distribution through a frequency-dependent separable kernel [11], [12].

For any admissible and analytic wavelet (*i.e.* we assume that $\text{supp}(F_\Psi(\omega)) = [0, +\infty[$ and $||F_\Psi(\omega)|| = 1$), then, the Plancherel theorem leads us to the frequency domain expression of the CWT, given by

$$\text{CW}_x(t,\omega) = \int_{\mathbb{R}} F_x(\Omega) F_\Psi(\frac{\omega_0 \Omega}{\omega})\, \mathbf{e}^{j\Omega t} \frac{d\Omega}{2\pi}. \tag{4}$$

Thus, we can now obtain the following reconstruction formula [11], [12] (Morlet formula)

$$x(t) = \frac{1}{C'_\Psi} \int_{\mathbb{R}} \text{CW}_x(t,\omega) \frac{\text{d}\omega}{|\omega|}, \tag{5}$$

where $C'_\Psi = \displaystyle\int_{\mathbb{R}} F_\Psi(\omega) \frac{\text{d}\omega}{|\omega|}$ is a proportionality factor. If x is real-valued, $x(t) = 2\text{Re}\left(\frac{1}{C'_\Psi} \displaystyle\int_0^{+\infty} \text{CW}_x(t,\omega) \frac{\text{d}\omega}{\omega} \right)$, can be used rather than Eq. (5).

A. Reassignment

Time-frequency reassignment [13] is a sharpening technique, which improves the localization of a TFR by moving its values to new coordinates which are closer to the real time-frequency support of the analyzed signal. For the CWT, it uses the reassignment operators which can be computed as follows [13]

$$\tilde{t}_{(t,\omega)} = t + \frac{\omega_0\ \text{CW}_x^{\mathcal{T}\Psi}(t,\omega)}{\omega\ \text{CW}_{x(t,\omega)}} \qquad \hat{t}(t,\omega) = \text{Re}\left(\tilde{t}(t,\omega)\right) \tag{6}$$

$$\tilde{\omega}_{(t,\omega)} = -\frac{\omega\ \text{CW}_x^{\mathcal{D}\Psi}(t,\omega)}{\omega_0\ \text{CW}_{x(t,\omega)}} \qquad \hat{\omega}(t,\omega) = \text{Im}\left(\tilde{\omega}(t,\omega)\right) \tag{7}$$

where $\text{CW}_x^{\mathcal{T}\Psi}(t,\omega)$ and $\text{CW}_x^{\mathcal{D}\Psi}(t,\omega)$ are two CWTs using the specific mother wavelet $\mathcal{T}\Psi(t) = t\Psi(t)$ and $\mathcal{D}\Psi(t) = \frac{d\Psi}{dt}(t)$.

Hence, a sharpened TFR also called reassigned scalogram, is obtained by moving the scalogram values to new coordinates according to $(t,\omega) \mapsto (\hat{t}(t,\omega), \hat{\omega}(t,\omega))$, which is computed as $\text{RCW}_x(t,\omega) =$

$$\iint_{\mathbb{R}^2} \left|\text{CW}_x(\tau,\Omega)\right|^2 \delta\left(t - \hat{t}(\tau,\Omega)\right) \delta\left(\omega - \hat{\omega}(\tau,\Omega)\right) d\tau\, d\Omega. \tag{8}$$

where $\delta(t)$ denotes the Dirac distribution. Despite a better localization, the resulting TFR is not reversible contrarily to the synchrosqueezing transform (*cf.* Section II-C).

B. Levenberg-Marquardt reassignment

New reassignment operators were proposed [9] and allow to adjust the energy localization in the time-frequency plane through a damping parameter μ. Finally, the Levenberg-Marquardt root finding algorithm leads us to new reassignment operators for CWT, which can be expressed as:

$$\begin{pmatrix} \hat{t}_\mu(t,\omega) \\ \hat{\omega}_\mu(t,\omega) \end{pmatrix} = \begin{pmatrix} t \\ \omega \end{pmatrix} - \left(\nabla^t R_x(t,\omega) + \mu I_2\right)^{-1} R_x(t,\omega) \tag{9}$$

$$R_x(t,\omega) = \begin{pmatrix} t - \hat{t}(t,\omega) \\ \omega - \hat{\omega}(t,\omega) \end{pmatrix} = \begin{pmatrix} -\text{Re}\left(\frac{\omega_0 \text{CW}_x^{\mathcal{T}\Psi}(t,\omega)}{\omega \text{CW}_x(t,\omega)}\right) \\ \omega + \text{Im}\left(\frac{\omega \text{CW}_x^{\mathcal{D}\Psi}(t,\omega)}{\omega_0 \text{CW}_x(t,\omega)}\right) \end{pmatrix} \tag{10}$$

$$\nabla^t R_x(t,\omega) = \begin{pmatrix} \frac{\partial R_x}{\partial t}(t,\omega) & \frac{\partial R_x}{\partial \omega}(t,\omega) \end{pmatrix} = \begin{pmatrix} \gamma_{11} & \gamma_{12} \\ \gamma_{21} & \gamma_{22} \end{pmatrix}$$

where I_2 is the 2×2 identity matrix. The elements of the matrix $\nabla^t R_x(t,\omega)$ are computed as:

$$\gamma_{11} = \frac{\partial}{\partial t}\left[-\text{Re}\left(\frac{\omega_0 \text{CW}_x^{\mathcal{T}\Psi}(t,\omega)}{\omega \text{CW}_{x(t,\omega)}} \right) \right] \tag{11}$$
$$= 1 + \text{Re}\left(\frac{\text{CW}_x^{\mathcal{T}\mathcal{D}\Psi}(t,\omega) \text{CW}_{x(t,\omega)} - \text{CW}_x^{\mathcal{T}\Psi}(t,\omega) \text{CW}_x^{\mathcal{D}\Psi}(t,\omega)}{\text{CW}_{x(t,\omega)^2}} \right)$$

$$\gamma_{21} = \frac{\partial}{\partial t}\left[\omega + \text{Im}\left(\frac{\omega \text{CW}_x^{\mathcal{D}\Psi}(t,\omega)}{\omega_0 \text{CW}_{x(t,\omega)}} \right) \right] \tag{12}$$
$$= \frac{\omega^2}{\omega_0^2} \text{Im}\left(\frac{\text{CW}_x^{\mathcal{D}\Psi}(t,\omega)^2 - \text{CW}_x^{\mathcal{D}^2\Psi}(t,\omega) \text{CW}_{x(t,\omega)}}{\text{CW}_{x(t,\omega)^2}} \right)$$

$$\gamma_{12} = \frac{\partial}{\partial \omega}\left[-\text{Re}\left(\frac{\omega_0 \text{CW}_x^{\mathcal{T}\Psi}(t,\omega)}{\omega \text{CW}_{x(t,\omega)}} \right) \right] \tag{13}$$
$$= \frac{1}{\omega^2} + \frac{\omega_0 - \omega}{\omega^2} \text{Re}\left(\frac{\text{CW}_x^{\mathcal{T}\Psi}(t,\omega)}{\text{CW}_{x(t,\omega)}} \right)$$
$$+ \text{Re}\left(\frac{\text{CW}_x^{D_\omega \mathcal{T}\Psi}(t,\omega) \text{CW}_{x(t,\omega)} - \text{CW}_x^{\mathcal{T}\Psi}(t,\omega) \text{CW}_x^{D_\omega \Psi}(t,\omega)}{\text{CW}_x(t,\omega)^2} \right)$$

$$\gamma_{22} = \frac{\partial}{\partial \omega}\left[\omega + \text{Im}\left(\frac{\omega \text{CW}_x^{\mathcal{D}\Psi}(t,\omega)}{\omega_0 \text{CW}_{x(t,\omega)}} \right) \right] = 1 + \text{Im}\left(\frac{\text{CW}_x^{\mathcal{D}\Psi}(t,\omega)}{\text{CW}_{x(t,\omega)}} \right) \tag{14}$$
$$+ \text{Im}\left(\frac{\text{CW}_x^{\mathcal{D}\Psi}(t,\omega)^2 - \text{CW}_x^{\mathcal{D}\Psi}(t,\omega) \text{CW}_{x(t,\omega)}}{\text{CW}_x(t,\omega)^2} \right)$$
$$+ \omega \text{Im}\left(\frac{\text{CW}_x^{D_\omega \mathcal{D}\Psi}(t,\omega) \text{CW}_x^{\mathcal{D}\Psi}(t,\omega) + \text{CW}_x^{D_\omega \Psi}(t,\omega) \text{CW}_x^{\mathcal{D}\Psi}(t,\omega)}{\text{CW}_x(t,\omega)^2} \right),$$

with $D_\omega \Psi(\frac{\omega}{\omega_0} t) = \frac{\partial}{\partial \omega}\left[\Psi(\frac{\omega}{\omega_0} t)\right]$, $D_\omega \mathcal{T}\Psi(\frac{\omega}{\omega_0} t) = \frac{\partial}{\partial \omega}\left[\mathcal{T}\Psi(\frac{\omega}{\omega_0} t)\right]$, and $D_\omega \mathcal{D}\Psi(\frac{\omega}{\omega_0} t) = \frac{\partial^2}{\partial \omega \partial t}\left[\Psi(\frac{\omega}{\omega_0} t)\right]$.

Thus, the Levenberg-Marquardt reassigned scalogram is simply obtained by replacing $(\hat{t}, \hat{\omega})$ by $(\hat{t}_\mu, \hat{\omega}_\mu)$ in Eq. (8).

C. Synchrosqueezed CWT

Synchrosqueezing [14] can be viewed as a variant of the reassignment method, which relocates the transform instead of its squared modulus to allow a signal reconstruction. In practice, it should be deduced from the CWT synthesis formula given by Eq. (5). Thus, the synchrosqueezed CWT can be defined as:

$$\text{S}_x(t,\omega) = |\omega| \int_{\mathbb{R}} \text{CW}_x(t,\omega') \delta\left(\omega - \hat{\omega}(t,\omega')\right) \frac{\text{d}\omega'}{|\omega'|}, \tag{15}$$

for which a sharpened TFR is provided by its squared modulus. Hence, this transform can be inverted by

$$\hat{x}(t) = \frac{1}{C'_\Psi} \int_{\mathbb{R}} \text{S}_x(t,\omega) \frac{\text{d}\omega}{|\omega|}. \tag{16}$$

For multicomponent signals, synchrosqueezing also allows to retrieve separately each mode by restricting the integration bounds in Eq. (16) to the corresponding frequency support of

this component. This support is assumed to be in the vicinity of a ridge which can be directly estimated from the TFR as proposed for example in [15].

D. Second-Order Synchrosqueezing

Second-order synchrosqueezing was first proposed by Oberlin *et al.* in [16] to improve TFRs of strongly modulated chirp signals. Assuming a signal model expressed as

$$x(t) = a(t)\,\mathrm{e}^{j\Phi(t)}, \text{ with } \Phi(t) = \varphi_x + \omega_x t + \alpha_x \frac{t^2}{2}, \quad (17)$$

where $a(t)$ and $\Phi(t)$ stand for the time-varying amplitude and phase.

Vertical synchrosqueezing uses an improved estimation of the instantaneous frequency (rather than the classical reassignment operator), thanks to a local modulation estimation $\tilde{q}$ which verifies $\hat{\alpha} = \mathrm{Im}(\tilde{q})$ (the reader can refer to [17] for details).

Thus, an improved instantaneous frequency estimator can be computed as

$$\hat{\omega}^{(2)}(t,\omega) = \begin{cases} \mathrm{Im}\left(\tilde{\omega}_{(t,\omega)} + \tilde{q}_{x(t,\omega)}(t - \tilde{t}_{(t,\omega)})\right) & \text{if } |\tilde{q}_{x(t,\omega)}| < \infty \\ \hat{\omega}(t,\omega) & \text{otherwise.} \end{cases} \quad (18)$$

Specifically to the CWT, an efficient local modulation estimator [18] provided by $\tilde{q}_x(t,\omega) = \frac{\frac{\partial \tilde{\omega}}{\partial t}(t,\omega)}{\frac{\partial \tilde{t}}{\partial t}(t,\omega)}$, can be used in Eq.(18). Finally, this definition with Eqs. (6) and (7), lead us to:

$$\tilde{q}_x(t,\omega) = \frac{\frac{\omega^2}{\omega_0^2}\left(\mathrm{CW}_x^{\mathcal{D}^2\Psi}{}_{(t,\omega)}\mathrm{CW}_x^{\Psi}{}_{(t,\omega)} - \mathrm{CW}_x^{\mathcal{D}\Psi}{}_{(t,\omega)}{}^2\right)}{\mathrm{CW}_x^{\mathcal{D}\Psi}{}_{(t,\omega)}\mathrm{CW}_x^{\mathcal{T}\Psi}{}_{(t,\omega)} - \mathrm{CW}_x^{\mathcal{T}\mathcal{D}\Psi}{}_{(t,\omega)}\mathrm{CW}_x^{\Psi}{}_{(t,\omega)}}, \quad (19)$$

which allows a direct computation through the CWT values, using the specific mother wavelet functions $\mathcal{D}^2\Psi(t) = \frac{\partial^2}{\partial t^2}\left[\Psi(t)\right]$ and $\mathcal{T}\mathcal{D}\Psi = t\mathcal{D}\Psi(t)$.

III. Recursive implementation

According to Eq. (3), the computation of $\mathrm{CW}_x(t,\omega)$ can also be viewed as a filtering operation which can be recursively implemented if we use for g a specific causal infinite impulse response filter, that corresponds to a modified version of the analysis window proposed in our previous work for the STFT [8], [19] (*cf.* Fig. 1):

$$g_k(t,s) = \frac{t^{k-1}}{(sT)^k(k-1)!}\,\mathrm{e}^{p\frac{t}{s}}\,U(t), \forall s>0, \quad (20)$$

$$\Psi_k(t) = g_k(-t,1)^* \quad (21)$$

with $p = -\frac{1}{T} + j\omega_0$, $k \geq 1$ being the filter order, T the time spread of the window and $U(t)$ the Heaviside step function.

The Fourier transform of the resulting impulse response g_k displayed in Fig. 1), can be expressed as

$$F_{g_k}(\omega) = \int_{\mathbb{R}} g_k(t,1)\,\mathrm{e}^{-j\omega t}dt = \frac{1}{(1+j(\omega-\omega_0)T)^k}, \quad (22)$$

and can be used to compute C'_Ψ which can be numerically approximated using the rectangle rule. Hence, the use of $g_k(t)$ is motivated by the fact that this window is a simple solution

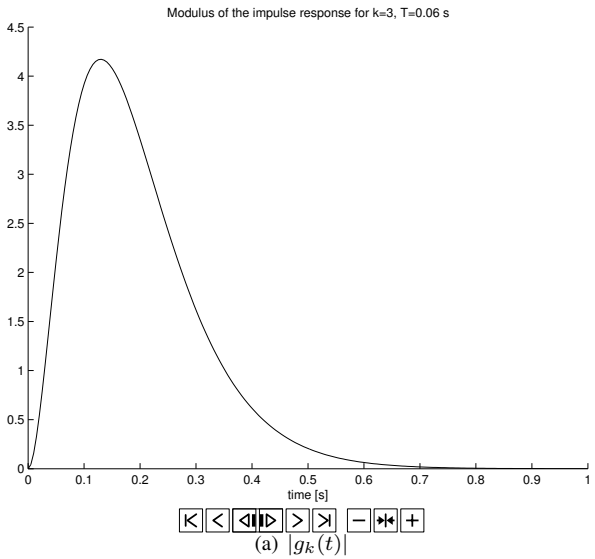

(a) $|g_k(t)|$

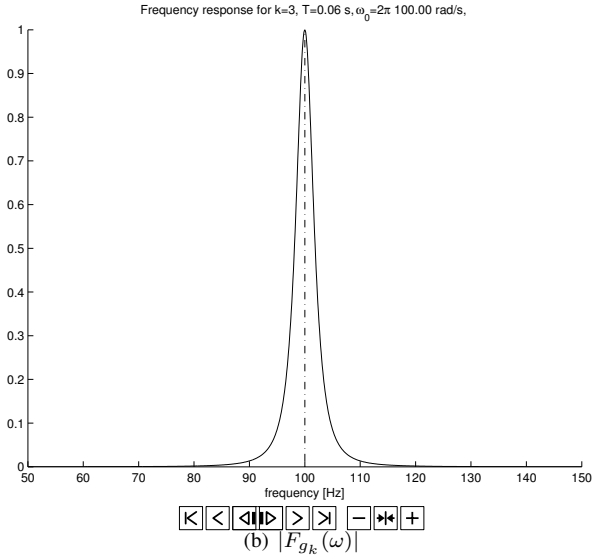

(b) $|F_{g_k}(\omega)|$

Fig. 1. Plot of the modulus of the analysis window $|g_k(t)|$ proposed in [8] (a) and of the frequency response of the resulting filter used for a recursive computation of the CWT with $\omega_0 = 2\pi 100$ rad.s^{-1} and $1/T_s = 1000$ Hz.

for an ordinary differential equation of the k-th order, which appears when Eq. (3) is differentiated with respect to time [19]. First, this property allows a discrete-time implementation in terms of a difference equation resulting from a recurrence equation. Second, this solution leads to simple relations between the different windows, when they are differentiated or multiplied by t^n ($\forall n \in \mathbb{N}$).

Using this definition, the partial derivatives with respect to frequency of Ψ_k given by Eq. (21), denoted D_ω in Eqs. (13) and (14), can now be substituted using:

$$D_\omega\Psi_k(\frac{\omega}{\omega_0}t) = \frac{1}{\omega}\left((k-1)\Psi_k(\frac{\omega}{\omega_0}t) + (j\omega_0 - \frac{1}{T})\mathcal{T}\Psi_k(\frac{\omega}{\omega_0}t)\right). \quad (23)$$

This leads to a computation through several recursive filters g_k, only involving differentiation with respect to time.

A. Discretization

Let $n \in \mathbb{Z}$ and $m = 0, 1, ..., M-1$ being respectively the discrete time and frequency indices for a sampling period T_s. Since $\omega_0 T = 2\pi f_0 T$, $\omega = \frac{2\pi m}{MT_s}$ and $t = nT_s$, the filter defined by Eqs. (3) and (20) can be computed as [8], using the impulse invariance method [20] as a function of $f_0 T$ as

$$G_k(z, \frac{\omega_0}{\omega}) = T_s \mathcal{Z}\left\{g_k(t, \frac{\omega_0}{\omega})\right\} = \frac{\sum_{i=0}^{k-1} b_i[m] z^{-i}}{1 + \sum_{i=1}^{k} a_i[m] z^{-i}}, \tag{24}$$

$$\text{with} \quad b_i[m] = \left(\frac{m}{f_0 T M}\right)^k \frac{1}{(k-1)!} B_{k-1,k-i-1} \alpha_m^i, \tag{25}$$

$$a_i[m] = A_{k,i} \left(-\alpha_m\right)^i, \text{ and } \alpha_m = \mathbf{e}^{(-\frac{1}{f_0 T} + j2\pi)\frac{m}{M}} \tag{26}$$

where $\mathcal{Z}\{f(t)\} = \sum_{n=0}^{+\infty} f(nT_s) z^{-n}$ is the z transform of $f(t)$, $B_{k,i} = \sum_{j=0}^{i} (-1)^j A_{k+1,j} (i+1-j)^k$ denotes the Eulerian numbers and $A_{k,i} = \binom{k}{i} = \frac{k!}{i!(k-i)!}$ the binomial coefficients.

Hence, $\text{CW}_k^g[n,m] \approx \text{CW}_x(nT_s, \frac{2\pi m}{MT_s})$ can be computed from the sampled analyzed signal $x[n]$ by a standard recursive equation expressed as:

$$\text{CW}_k^g[n,m] = \sum_{i=0}^{k-1} b_i[m]\, x[n-i] - \sum_{i=1}^{k} a_i[m]\, \text{CW}_k^g[n-i,m]. \tag{27}$$

The z transform of the other specific impulse responses can be expressed as functions of $G_k(z, \frac{\omega_0}{\omega})$ at different orders using the relation $\Psi_k(\frac{\omega t}{\omega_0}) = \frac{\omega_0}{\omega} g_k(t, \frac{\omega_0}{\omega})$ and the properties expressed below [8]:

$$T_s \mathcal{Z}\{\mathcal{T} g_k(t,s)\} = kT\ G_{k+1}(z,s) \tag{28}$$

$$T_s \mathcal{Z}\left\{\mathcal{D} g_k(t,s)\right\} = \frac{1}{T}\ G_{k-1}(z,s) + p\ G_k(z,s) \tag{29}$$

$$T_s \mathcal{Z}\left\{\mathcal{D}\mathcal{T} g_k(t,s)\right\} = k\left(G_k(z,s) + pT\ G_{k+1}(z,s)\right) \tag{30}$$

$$\begin{aligned} T_s \mathcal{Z}\left\{\mathcal{T}\mathcal{D} g_k(t,s)\right\} &= T_s \mathcal{Z}\left\{\mathcal{D}\mathcal{T} g_k(t,s) - g_k(t,s)\right\} \\ &= (k-1)\ G_k(z,s) + kpT\ G_{k+1}(z,s) \end{aligned} \tag{31}$$

$$T_s \mathcal{Z}\left\{\mathcal{T}^2 g_k(t,s)\right\} = k(k+1)T^2\ G_{k+2}(z,s) \tag{32}$$

$$\begin{aligned} T_s \mathcal{Z}\left\{\mathcal{D}^2 g_k(t,s)\right\} &= \frac{1}{T^2}\ G_{k-2}(z,s) + \frac{2p}{T}\ G_{k-1}(z,s) \\ &\quad + p^2\ G_k(z,s). \end{aligned} \tag{33}$$

These results hold for any $k \geq 1$ provided that $G_0(z,s) = G_{-1}(z,s) = 0$. Eqs. (28) and (29) generalize to any value of k some results already presented in [19], while Eqs. (30) to (33) provide the discrete-time linear systems required by the Levenberg-Marquardt reassignment operators and the second-order vertical synchrosqueezing.

B. Practical recursive implementation

Considering a sampled discrete-time signal $x[n] \approx x(nT_s)$, the recursive discrete-time CWT is computed using the difference equation given by (27).

The CWTs using the specific mother wavelet functions required to compute the reassignment operators are recursively computed thanks to the relations between the different filters provided by Eqs. (28)-(33).

Thus, the recursive implementation can be summarized by the following procedure.

1) Compute the required $\text{CW}_k^g[n,m]$ using $x[n-i]$ and $\text{CW}_k^g[n-l,m]$ with $i \in [0, k-1]$, $l \in [1, k]$
2) Compute the other required specific filtered signals (*i.e.* $\text{CW}_k^{\mathcal{T}g}$, $\text{CW}_k^{\mathcal{D}g}$, $\text{CW}_k^{\mathcal{D}\mathcal{T}g}$, $\text{CW}_k^{\mathcal{T}^2 g}$ or $\text{CW}_k^{\mathcal{D}^2 g}$) using CW_k^g with different filter orders
3) Compute the discrete-time reassignment operators defined as $\hat{n} = \frac{\hat{t}}{T_s}$ and $\hat{m} = \frac{\hat{\omega} M T_s}{2\pi}$
4) **If** $\hat{n} \leq n$ **then** update $\text{TFR}[\hat{n}, m]$ **else** store the triplet $(\text{CW}_k^g[n,m], \hat{n}, m)$ into a list
5) Update $\text{TFR}[n,m]$ using all previously stored triplets such as $\hat{n} = n$ and remove them from the list

IV. Computation on a synthetic signal

Fig. 2 compares the new proposed recursive TFRs corresponding to the CWT with those provided by the recursive STFT proposed in [8], [17]. For this, we use a 500 samples long multicomponent real signal made of two impulses, one sinusoid, one chirp, one sinusoidally modulated sinusoid and a white Gaussian noise with a Signal-to-Noise Ratio (SNR) equal to 25 dB. To make our results comparable between the CWT and the STFT, our computations use $M = 500$, $k = 7$ and we define for both transforms the same window spread $L = \frac{T}{T_s} = 6$, and a central normalized frequency $\lambda_0 = 0.2$ which leads to $f_0 T = \lambda_0 L = 1.2$.

These figures illustrate the advantage of the CWT compared to the STFT to localize the two impulses and the time-varying components. For each transform, the reassigned and synchrosqueezed versions clearly illustrate the improvement of the signal components localization compared to the initial TFR. As expected, the reassigned TFRs obtains the best time-frequency localization, while the Levenberg-Marquardt approach requires a fine candidate of its damping parameter μ. The recursive synchrosqueezed CWT and STFT which are invertible, also provide an efficient time-frequency localization which is further improved by vertical synchrosqueezing, except for the impulse signals. The reconstruction quality of the analyzed signal is measured in terms of Reconstruction Quality Factor (RQF), defined as [8]

$$\text{RQF} = 10 \log_{10}\left(\frac{\sum_n |x[n]|^2}{\sum_n |x[n] - \hat{x}[n]|^2}\right). \tag{34}$$

In this simulation, the CWT obtains poorer RQFs than the STFT. This can be explained since our computations use a linear scale for the frequencies and the result is a constant frequency resolution which advantages the STFT over the CWT for signal reconstruction. This issue could be compensated for the CWT if a logarithmic scale is used.

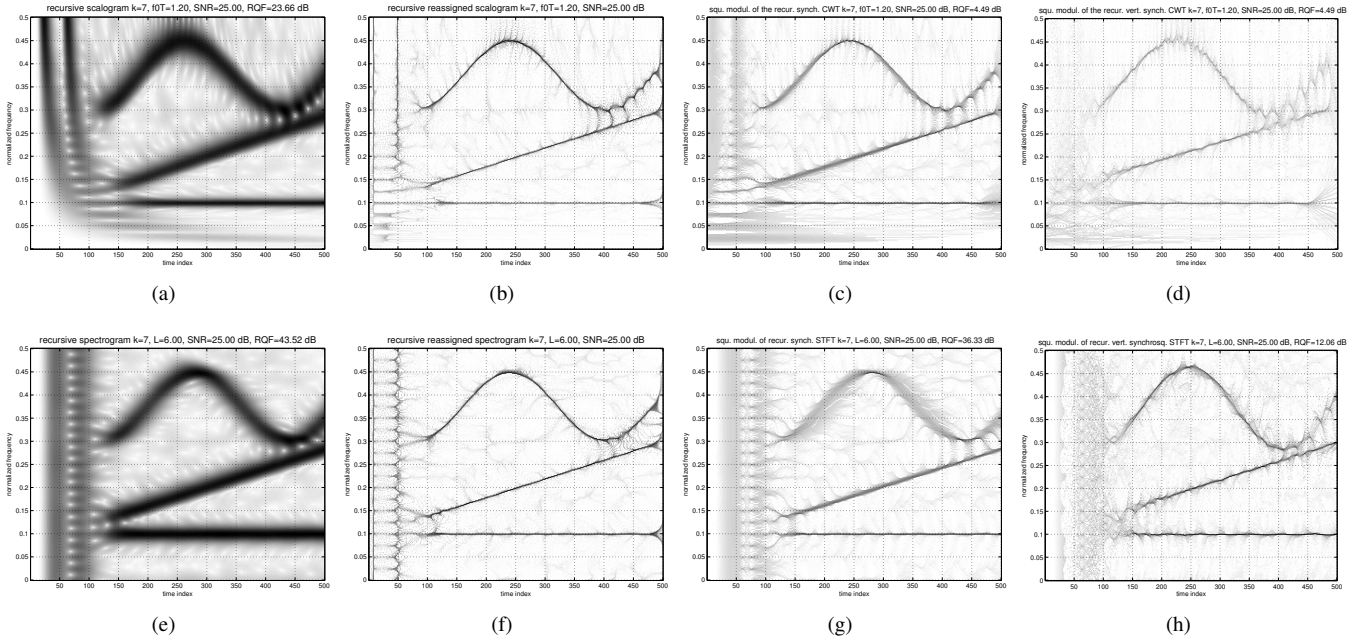

Fig. 2. TFRs comparison between (a) the recursive scalogram, (b) the recursive reassigned scalogram, (c) the squared modulus of the synchrosqueezed CWT, (d) the squared modulus of the vertically synchrosqueezed CWT, (e) the recursive spectrogram, (f) the recursive reassigned spectrogram, (g) the squared modulus of the synchrosqueezed STFT, (h) the squared modulus of the vertically synchrosqueezed STFT.

V. Conclusion

We have proposed a new mother wavelet function allowing a recursive implementation of the CWT through causal IIR filtering. We have also introduced a specific formulation of the Levenberg-Marquardt reassignment operators designed for the CWT, which is also valid for the non-recursive version of the CWT. Thus, these new tools for which MATLAB codes are available on-line [21], [22], pave the way of real-time implementation of sharpen and invertible TFRs comparable to the CQT [1]. In future work, we will complete a further investigation of these new proposed tools in terms of efficiency, from a theoretical point of view, but also from a practical point of view by considering potential application scenarios.

References

[1] J. C. Brown, "Calculation of a constant Q spectral transform," *The Journal of the Acoustical Society of America*, vol. 89, no. 1, pp. 425–434, 1991.

[2] R. G. Stockwell, L. Mansinha, and R. P. Lowe, "Localization of the complex spectrum: the S-transform," *IEEE Trans. Signal Process.*, vol. 44, no. 4, pp. 998–1001, Apr. 1996.

[3] P. Flandrin, *Time-Frequency/Time-Scale analysis*. Acad. Press, 1998.

[4] T. Chi, P. Ru, and S. A. Shamma, "Multiresolution spectrotemporal analysis of complex sounds," *The Journal of the Acoustical Society of America*, vol. 118, no. 2, pp. 887–906, 2005.

[5] J. Andén and S. Mallat, "Multiscale scattering for audio classification." in *Proc. ISMIR*, 2011, pp. 657–662.

[6] J. Ganseman, P. Scheunders, and S. Dixon, "Improving PLCA-based score-informed source separation with invertible constant-Q transforms," in *Proc. EUSIPCO*, Bucharest, Romania, 2012, pp. 2634–2638.

[7] S. Mallat, *A wavelet tour of signal processing*. Academic press, 1999.

[8] D. Fourer, F. Auger, and P. Flandrin, "Recursive versions of the Levenberg-Marquardt reassigned spectrogram and of the synchrosqueezed STFT," in *Proc. IEEE ICASSP*, Mar. 2016, pp. 4880–4884.

[9] F. Auger, E. Chassande-Mottin, and P. Flandrin, "Making reassignment adjustable: the Levenberg-Marquardt approach," in *Proc. IEEE ICASSP*, Mar. 2012, pp. 3889–3892.

[10] A. Grosssmann and J. Morlet, "Decomposition of Hardy functions into square integrable wavelets of constant shape," *IAM Journal of Mathematical Analysis*, vol. 15, no. 4, pp. 723–736, 1984.

[11] D. Fourer, F. Auger, and J. Hu, "Reassigning and synchrosqueezing the Stockwell transform: Complementary proofs," Tech. Rep., Dec. 2015. [Online]. Available: http://hal.archives-ouvertes.fr/hal-01467244

[12] A. T. Poyil, S. Aljahdali, and N. KM, "Significance of Cohen's class for time frequency analysis of signals," *International Journal of Computer Applications*, vol. 72, no. 12, 2013.

[13] F. Auger and P. Flandrin, "Improving the readability of time-frequency and time-scale representations by the reassignment method," *IEEE Trans. Signal Process.*, vol. 43, no. 5, pp. 1068–1089, May 1995.

[14] I. Daubechies and S. Maes, "A nonlinear squeezing of the continuous wavelet transform," *Wavelets in Medecine and Bio.*, pp. 527–546, 1996.

[15] E. Brevdo, N. S. Fuckar, G. Thakur, and H.-T. Wu, "The synchrosqueezing algorithm: a robust analysis tool for signals with time-varying spectrum," *Arxiv preprint*, 2011.

[16] T. Oberlin, S. Meignen, and V. Perrier, "Second-order synchrosqueezing transform or invertible reassignment? Towards ideal time-frequency representations," *IEEE Trans. Signal Process.*, vol. 63, no. 5, pp. 1335–1344, Mar. 2015.

[17] D. Fourer, F. Auger, K. Czarnecki, S. Meignen, and P. Flandrin, "Chirp rate and instantaneous frequency estimation: application to recursive vertical synchrosqueezing," *IEEE Signal Process. Lett.*, Jun. 2017.

[18] T. Oberlin and S. Meignen, "The second-order wavelet synchrosqueezing transform," in *Proc. IEEE ICASSP*, Mar. 2017.

[19] G. K. Nilsen, "Recursive time-frequency reassignment," *IEEE Trans. Signal Process.*, vol. 57, no. 8, pp. 3283–3287, Aug. 2009.

[20] L. Jackson, "A correction to impulse invariance," *IEEE Signal Process. Lett.*, vol. 7, no. 10, pp. 237–275, October 2000.

[21] "ASTRES project MATLAB resources," http://www.ens-lyon.fr/PHYSIQUE/Equipe3/ANR_ASTRES/resources.html.

[22] D. Fourer, J. Harmouche, J. Schmitt, T. Oberlin, S. Meignen, F. Auger, and P. Flandrin, "The ASTRES toolbox for mode extraction of non-stationary multicomponent signals," in *Proc. EUSIPCO*, Kos island, Greece, Aug. 2017.